Cement and Concrete Research 39 (2009) 1044–1051

Contents lists available at ScienceDirect

Cement and Concrete Research

journal homepage: http://ees.elsevier.com/CEMCON/default.asp

Dynamic behaviour and visco-elastic damage model of ultra-high performance cementitious composite

Jianzhong Lai [a,*], Wei Sun [b]

[a] Department of Materials Science and Engineering, Nanjing University of Science and Technology, Nanjing 210094, PR China
[b] College of Materials Science and Engineering, Southeast University, Nanjing 211189, PR China

ARTICLE INFO

Article history:
Received 13 October 2008
Accepted 15 July 2009

Keywords:
Cement composite
Mechanical properties
Fiber reinforcement
Modeling

ABSTRACT

The dynamic behaviour of ultra-high performance cementitious composite (UHPCC) with compressive strength of 200 MPa with different steel fiber volume fractions was studied under impact using the split Hopkinson pressure bar. Three aspects of the testing: a gimbal device, wave shaping and direct strain measurement, were used to increase experimental accuracy. Results indicate that UHPCC has obvious strain rate effects. The peak stress, peak strain, elastic modulus and the area under the stress–strain curve increase with increasing strain rate. When the strain rate exceeds a threshold value, specimens with and without fibers begin to fracture. At high strain rate the unreinforced specimens fracture into small parts while fiber reinforced ones only have fine cracks on the edges. A visco-elastic damage model of UHPCC is proposed based on a nonlinear visco-elastic model (the ZWT model) and the material damage measured by the ultrasonic wave velocity method.

1. Introduction

Ultra-high performance cementitious composite (UHPCC) is a type of building material with very high strength and durability. Its high strength and ductility make it suitable for bridge decks, thin shell structures, nuclear power plants and defensive facilities that may experience impact loads [1–4]. A great number of tests have been conducted to find the effect of strain rate on the dynamic strength of concretes. The split Hopkinson pressure bar (SHPB) is an effective method to obtain the dynamic stress–strain curves of materials. Grote et al. studied the behaviour of concrete and mortar with strain rates between 250 and 1700/s by SHPB, and Ross et al. tested several cylindrical concrete specimens with diameters from 19 to 51 mm by SHPB in direct tension, splitting tension, and direct compression [5,6]. It is generally accepted that there is an apparent increase of the strength when normal strength concretes are subjected to dynamic loads.

In this paper, UHPCC was prepared by replacing 60% of cement with ultra-fine industrial waste powder. The dynamic behaviour of UHPCC was studied through SHPB and the damage of UHPCC was measured by ultrasonic wave velocity method at different strain rates. A constitutive model including strain rate is required to design structures subjected to impact. Based on a nonlinear visco-elastic model and the material damage, a visco-elastic damage model of UHPCC was proposed and the accuracy of this model was compared to experimental results.

2. Materials preparation

Four cementitious materials were used in the preparation of UHPCC including Portland cement, silica fume, fly ash and blast-furnace slag. The strength grade of cement is P·II 52.5 according to the relevant Chinese standard. The maximum particle size of natural sand is 2.5 mm with a fineness modulus of 2.6. The polycarboxylate based superplasticizer was used and its characterization is given in Table 1. The equivalent diameter, length and tensile strength of the steel fiber are 0.2 mm, 13 mm and 1800 MPa respectively.

The mix proportion and static uniaxial compressive strength of UHPCC with different steel fiber fractions are listed in Table 2. The cementitious materials and sand were put in a forced mortar mixer at the same time and mixed for 3 min. The water and superplasticizer were mixed together and then added into the mixer, and mixed for a further 6 min. Finally, fibers were added and mixed for 3 min to ensure that they were well distributed in the mortar. After mixing, the UHPCC was cast into steel moulds and compacted on a standard vibrating table. The specimens were stored in the standard conditions (20 °C ± 2 °C, R.H.>90%) and demoulded after 24 h. Then the specimens were cured in the standard conditions for 60 days before testing.

3. Experimental method of impact

The cylindrical specimens for SHPB test were 70 mm in diameter and 35 mm in length. A typical SHPB set-up is outlined in Fig. 1. It is composed of elastic input and output bars with a short specimen placed between them. The impact of the projectile at the free end of

* Corresponding author. Tel.: +86 025 84303881.
E-mail address: jzh-lai@163.com (J. Lai).

0008-8846/$ – see front matter © 2009 Elsevier Ltd. All rights reserved.
doi:10.1016/j.cemconres.2009.07.012

Table 1
Characteristics of polycarboxylate based superplasticizer.

Characteristics	Values
Solids content (%)	42
pH	7.1
Density (g/cm^3)	1.13
Cl (%)	0.02
Alkali (%)	1.58

the input bar develops a compressive longitudinal incident wave $\varepsilon_i(t)$. Once this wave reaches the interface of the bar and the specimen, a part of it $\varepsilon_r(t)$, is reflected, whereas another part goes through the specimen and transmits to the output bar $\varepsilon_t(t)$. These three basic waves are recorded by the gauges pasted on the input and output bars. According to the wave propagation theory, the average stress, strain and strain rate of specimens can be calculated by the following equation:

$$\sigma = E_0\varepsilon_t(t)\frac{A_0}{A_s},\ \dot{\varepsilon} = \frac{2C_0}{L_s}[\varepsilon_i(t) - \varepsilon_t(t)],\ \varepsilon = \int_0^t \dot{\varepsilon}\ (t)dt \quad (1)$$

where, E_0 and C_0 are the Young's modulus and the elastic wave speed of the bar. A_0 and A_s are the cross sectional areas of the bar and the specimen, and L_s is the length of the specimen.

In this study the SHPB test has been improved in three ways: including a gimbal device, pulse shaping, and direct strain measurement.

(1) Gimbal device

The two impact sides of the specimen must be parallel to increase the accuracy of the test. The unparallel sides will lead to local failure in the specimen and inaccuracy in strain measurement so the two sides of the specimen are polished to insure parallelism and are coated with Vaseline to reduce friction. The uneven contact between the bar and the specimen lasts a very short time on impact, so it has few effects on metal or polymer which are easily deformable. However it has obvious effects on brittle cementitious composites which crack at low strain. To avoid uneven contact and stress concentration in the specimen, a gimbal device is placed between the input bar and the specimen (Fig. 2). The gimbal device is a column with the same material and diameter as the bar. The gimbal device is cut into two parts by the spherical surface and adjusts automatically on the impact to insure the even contact between the bar and the specimen.

(2) Pulse shaping

The stress in the specimen is not distributed equally in the traditional SHPB test. Therefore, the shape of the incident wave has been designed to evenly distribute the stress in the specimen and make the strain rate approximately constant. Fig. 3 shows the pulse shaping in SHPB test. A piece of easily deformed circular metal, such as copper, is glued to the impact side of the input bar. The brittle specimen is usually damaged in the rising slope if it is impacted by a rectangular incident wave. Therefore, there is not enough time to achieve equal stress distribution in the specimen before it is damaged.

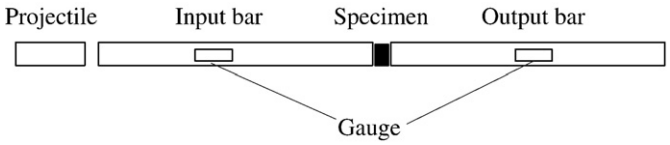

Fig. 1. SHPB test.

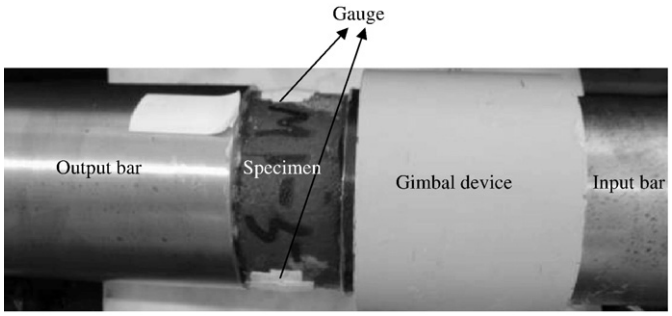

Fig. 2. Placement of gimbal device.

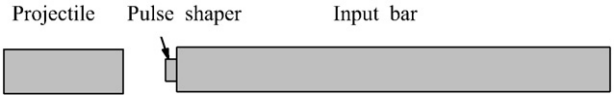

Fig. 3. Method of pulse shaping.

As shown in Fig. 4, the pulse shaper can eliminate high frequent loading wave and change the rectangular wave into triangular wave. The time for the rising of the incident wave is extended and the loading rate is reduced, so even stress and strain in specimen is obtained.

(3) Direct strain measurement

The stress and strain of the specimen are calculated from the stress waves recorded by the gauges on the SHPB bars. But the initial strain of the specimen was not accurate in the traditional SHPB test. In the present research, the initial strain is measured directly by two gauges glued symmetrically on the surface of the specimen (Fig. 2). The initial elastic modulus of the specimen is calculated from the strain measured directly and the stress is deduced from Eq. (1). After the specimen cracks and the gauges on it split, the strain of the specimen is deduced from Eq. (1).

4. Results and analysis

4.1. Stress waves on impact

Fig. 5 shows the stress waves through the same material ($UPCV_4$) at different impact speeds. Results indicate that three types of waves increase with increasing impact speed. Eq. (1) shows that the stress of the specimen is proportional to the amplitude of the transmitted

Table 2
Mix proportions of UHPCC.

Materials	Binder (wt.%)				Fiber volume fraction	Superplasticizer/binder	Sand/binder	Water/binder	Static compressive strength
	Cement	Silica fume	Fly ash	Slag	(%)				(MPa)
$UPCV_0$	40	10	25	25	0	0.02	1.2	0.16	143
$UPCV_3$	40	10	25	25	3	0.02	1.2	0.16	186
$UPCV_4$	40	10	25	25	4	0.02	1.2	0.16	204

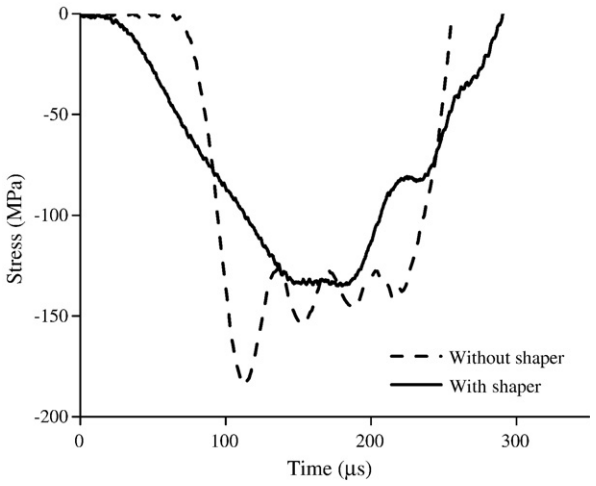

Fig. 4. Incident waves with and without pulse shaper.

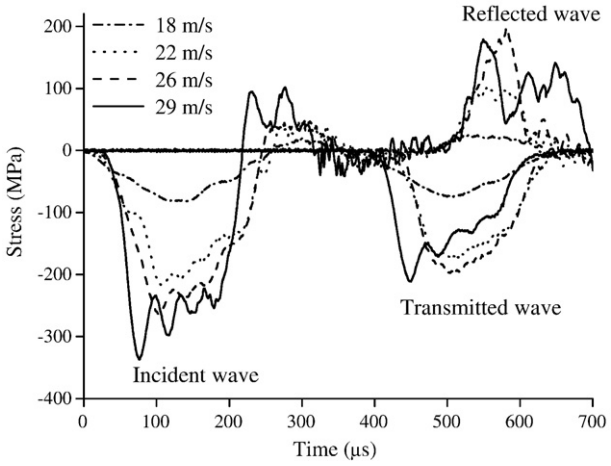

Fig. 5. Stress waves through UPCV4 at different impact speeds.

wave and the strain of the specimen is in proportion to the area under the reflected wave, so the stress and strain of the specimen increase with increasing impact speed. Fig. 6 shows the stress waves through three UHPCCs at the same impact speed. Results indicate that the

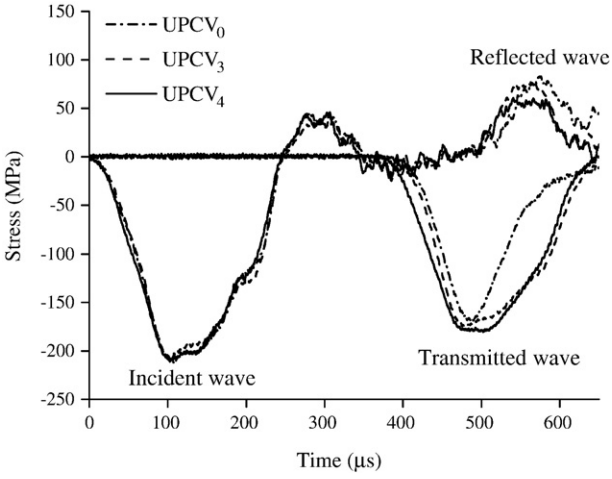

Fig. 6. Stress waves through different materials at impact speed of 22 m/s.

incident waves through different materials are very similar at the same impact speed but the areas under the transmitted waves are different. The areas under the transmitted waves represent the energy absorbed by the specimen on the impact. The area under the transmitted waves of fiber reinforced specimens ($UPCV_3$ and $UPCV_4$) is larger than that of the unreinforced specimen ($UPCV_0$), showing the ability of the reinforced specimen to absorb higher amounts of energy.

4.2. Dynamic properties of UHPCC at different strain rates

Fig. 7 shows the stress–strain curves of UHPCC at different strain. Table 3 indicates the dynamic properties of UHPCC. Results show that UHPCC has obvious strain rate effect. The material peak stress, peak strain and elastic modulus increase with increasing strain rate. The peak stress, peak strain and elastic modulus of fiber reinforced UHPCC were higher than those of unreinforced UHPCC at similar strain rates. The areas under the stress–strain curves represent the work of impact load and the areas are an indication of the toughness of materials. Table 3 shows that the impact toughness of UHPCC increases as strain rate increases. The toughness of UHPCC is also improved by steel fiber reinforcement. Table 3 shows that the peak strain increases with fiber volume fraction. As shown in Fig. 7, the effect of fiber volume fraction is less on the rising stage than on the descending stage of the stress–strain curve: the descending stress–strain curve falls more slowly with fiber reinforcement.

There is an obvious effect of steel fiber reinforcement on the static strength of UHPCC and the effect increases with the increase of fiber volume fraction while the effect of fiber volume fraction on the dynamic strength of UHPCC is reduced at high strain rate. On the one hand, the different effects of steel fiber reinforcement on the static and dynamic strength come from the difference between the static and dynamic fracture pattern of UHPCC. Under static loading, the specimen breaks laterally along the diameter and there is one major crack across the weak zones of the specimen. The bridge effect of fibers is great in this static fracture pattern. Under dynamic loading, many cracks appear in the concrete and the specimen is fractured into many small fragments. Fibers are pulled out from the matrix and their bridge effects are reduced. On the other hand, the fiber reinforced UHPCC does not completely disintegrate because of the high strength of UHPCC and the insufficient energy present in the SHPB.

The strain rate sensitivity of concrete is usually ascribed to two causes: the time-dependent movement of free water in the matrix through voids and pores, and the time-dependent nature of crack growth relative to the load rate [7]. The importance of moisture is not always recognized in research resulting in a wide scatter in the reported results. However, like the creep of concrete, the strain rate sensitivity of concrete is greatest when it is fully saturated and least when it is dry. A crack requires a finite time to propagate, therefore time-dependent effects plays a role in strain rate effect. Crack velocity increases with the increase of strain rate, but remains much smaller than that of stress wave in concrete. At high rates of loading, when cracks propagate much more slowly than the applied stress, the crack path is altered and the crack length is shortened, which translates into improved compressive, tensile and fracture properties at increasing load rates [7].

Similarly to the work of Bracc and Joncs [8] and Janach [9] on the strain rate effect on rocks, the strain rate effect of UHPCC can also be seen as the mechanical behaviour in the transition from the uniaxial stress state to the uniaxial strain state. In the SHPB test, the specimen is not completely in the uniaxial stress state because of the large size of the specimen. Especially in the middle of the specimen, the radial strain is confined due to the material inertia. The higher the strain rate is, the stronger the confinement is. Therefore the dynamic strength increases with the increase of strain rate, as if the material is in triaxial compression. Gorham analyzed inertial effects of specimens and

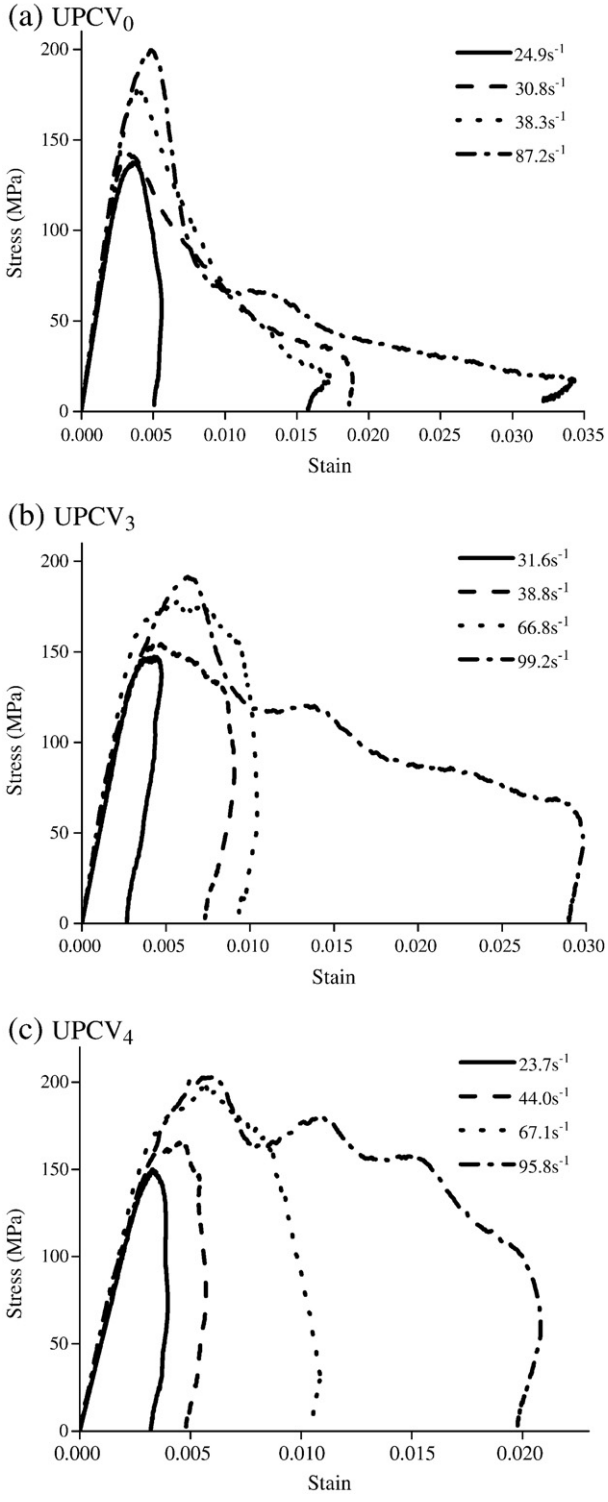

Fig. 7. Stress–strain curves of UHPCC at different strain rates.

proposed a formula (Eq. (2)) to calculate $\Delta\sigma$, the difference between experimental and true stress [10].

$$\Delta\sigma = \rho_s\left(\frac{a^2}{8} + \frac{h^2}{12}\right)\frac{d\dot{\varepsilon}}{dt} + \rho_s\left(\frac{h^2}{12} - \frac{a^2}{16}\right)\dot{\varepsilon}^2 \quad (2)$$

where, ρ_s, a and h are the density, radius and length of the specimen. $\dot{\varepsilon}$ is strain rate. Strain rates are approximately constant in present SHPB tests using pulse shaping, hence $\frac{d\dot{\varepsilon}}{dt} = 0$. If $\frac{h}{a} = \frac{\sqrt{3}}{2}$, then $\frac{h^2}{12} - \frac{a^2}{16} = 0$. Therefore, inertial effects can be reduced by loading in constant strain rate and designing specimen sizes proportionably.

Table 3
Dynamic properties of UHPCC at different strain rates.

Materials	Strain rate	Elastic modulus	Peak strain	Peak stress	Area under stress–strain curve
	(s^{-1})	(GPa)	($\times 10^{-6}$)	(MPa)	(MPa)
$UPCV_0$	24.9	50.1	3588	138	0.507
	30.8	53.9	3340	142	1.345
	38.3	52.8	3923	178	1.397
	87.2	58.0	4883	200	2.096
$UPCV_3$	31.6	47.3	4290	147	0.331
	38.8	49.6	4421	155	1.007
	66.8	53.7	5575	178	1.419
	99.2	57.4	6308	192	3.145
$UPCV_4$	23.7	51.8	3281	150	0.342
	44.0	55.7	4619	175	0.621
	67.1	57.2	5570	199	1.498
	95.8	60.2	5808	203	3.037

Fiber orientation is an important factor of the strength of discontiguous fibers reinforced concrete. The cosine of the angle between fiber orientation and loading direction indicates the efficiency of fiber reinforcement [11]. When fiber orientations are parallel to loading direction, the average efficiency of fibers reinforcement is 1.0. When fiber orientations are vertical to loading direction, the average efficiency is zero. For three-dimensional random fiber orientation, the average efficiency is 0.5 [11]. For relatively small specimens, as required by the Hopkinson apparatus, it is very difficult to get a truly random fiber orientation. Therefore, the dynamic strength of the specimen is higher when fiber orientation is parallel to the direction of loading than that when fiber orientation is random.

4.3. The fracture pattern of UHPCC at different strain rates

Fig. 8 shows the typical fracture pattern of specimens at high strain rate, and show that the damage to fiber reinforced UHPCC was much less than that of unreinforced UHPCC at similar strain rates. Fig. 8 also shows that unreinforced specimens break into small pieces while specimens with fibers remain unbroken on impact. The width and depth of the cracks in the specimens decreased with increasing fiber content. The randomly distributed fine fibers in UHPCC form networks to prevent the matrix from breaking. As a result, the damage of fiber reinforced specimens is lessened on high speed impact.

Fig. 8 shows that neither specimens with nor without fibers had any visible damage when the strain rates were below a threshold values. Small cracks appear on the side of $UPCV_4$ specimen at a strain rate over 60/s while the edge of unreinforced specimens is cracked at a strain rate over 30/s. The number of the cracks on the edge of $UPCV_4$ increases at strain rates over 90/s while $UPCV_0$ is broken into several parts of different size at strain rate over 40/s and into small pieces over 80/s. Results indicate that fiber reinforced UHPCC cracks slightly yet remains unbroken at high strain rate.

5. Visco-elastic damage model of UHPCC

5.1. Nonlinear visco-elastic model

Researching the dynamic behaviour of engineering plastic, Zhu, Wang and Tang proposed a nonlinear visco-elastic model — the ZWT model [12,13]. As shown in Fig. 9, the model is composed of a nonlinear elastic spring, a low frequency Maxwell element and a high

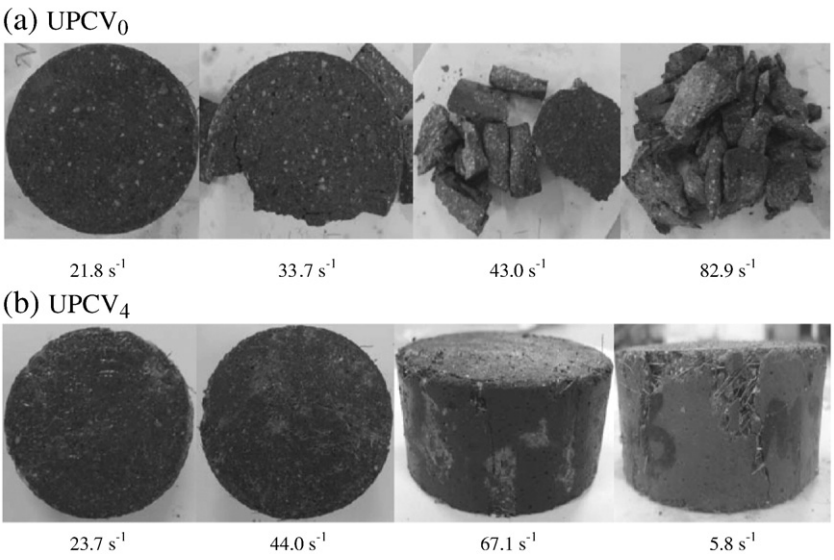

Fig. 8. Fracture pattern of UHPCC at different strain rates.

frequency Maxwell element. The formulation of ZWT model is as follows:

$$\sigma = f_e(\varepsilon) + E_1 \int_0^t \dot{\varepsilon} \exp\left(-\frac{t-\tau}{\theta_1}\right) d\tau + E_2 \int_0^t \dot{\varepsilon} \exp\left(-\frac{t-\tau}{\theta_2}\right) d\tau \quad (3)$$

where

$$f_e(\varepsilon) = E_0\varepsilon + \alpha\varepsilon^2 + \beta\varepsilon^3 \quad (4)$$

$f_e(\varepsilon)$ is the function of strain ε and describes the nonlinear elastic behaviour of the material. E_0, α and β are elastic constants. τ is the time variable and t is the loading time. The first integral term describes the visco-elastic behaviour at low strain rate while the second describes material behaviour at high strain rate. E_1 and θ_1 are the elastic constant and relaxation time of the low frequency Maxwell element respectively while E_2 and θ_2 are those of the high frequency one.

The time of loading is from 1 s to 10^2 s in the quasi-static state. The relaxation time (θ_2) is from 1 μs to 102 μs, so the high frequency Maxwell element relaxes at the beginning of loading [14]. Therefore, Eq. (3) becomes

$$\sigma = f_e(\varepsilon) + E_1 \int_0^t \dot{\varepsilon} \exp\left(-\frac{t-\tau}{\theta_1}\right) d\tau \quad (5)$$

On the contrary, for impact loading, the time of loading is from 1 μs to 102 μs. The relaxation time (θ_1) is from 10 s to 10^2 s, so there is no enough time for the low frequency Maxwell element to relax. Therefore, Eq. (3) becomes

$$\sigma = f_e(\varepsilon) + E_1\varepsilon + E_2 \int_0^t \dot{\varepsilon} \exp\left(-\frac{t-\tau}{\theta_2}\right) d\tau \quad (6)$$

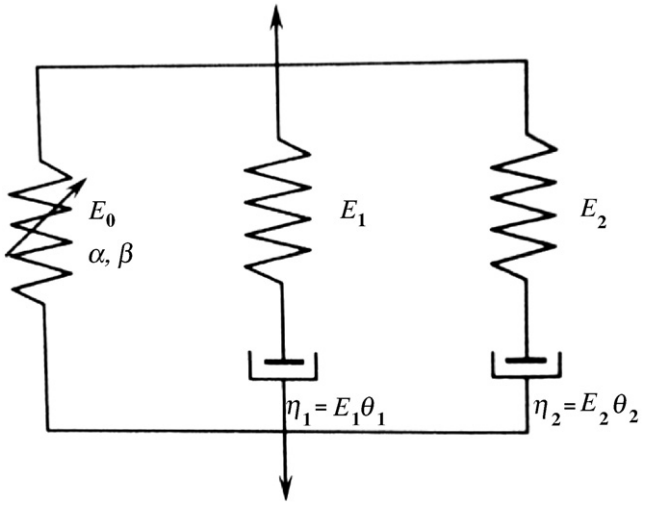

Fig. 9. Nonlinear visco-elastic model.

5.2. Visco-elastic damage model of UHPCC

Results indicate that UHPCC has obvious strain rate effect on impact. A modified ZWT model is used to describe the constitutive relation of UHPCC. Damage is an important factor in the constitutive model of concrete, so it is necessary for the dynamic model of UHPCC to include damage variable. The wave velocities V in the UHPCC specimen were measured by ultrasonic wave velocity method. This method consists of measuring the travel time of a pulse of longitudinal ultrasonic wave passing through the concrete. As shown in Fig. 10, The transmitter sends a pulse and it travels through the concrete specimen and reaches the receiver. The travel times between the initial onset and reception of the pulse are measure electronically. The path length between the transmitter and receiver divided by the time of travel gives the average velocity of wave propagation. The interfaces of the transducers and the specimens were coated with butter to ensure good coupling. The material damage D at different strain rate is defined as [15,16]:

$$D = 1 - \frac{E_1}{E_0} = 1 - \frac{V_1^2}{V_0^2} \quad (7)$$

where, E_0 is the initial elastic modulus and V_0 is the initial ultrasonic wave velocity of the specimen. E_1 is the elastic modulus and V_1 is the ultrasonic wave velocity of the specimen after impact.

Fig. 11 shows that the damage of UHPCC increases in proportion to the strain rate. The linear relationship between the damage D and the strain rate $\dot{\varepsilon}$ is found by linear regression.

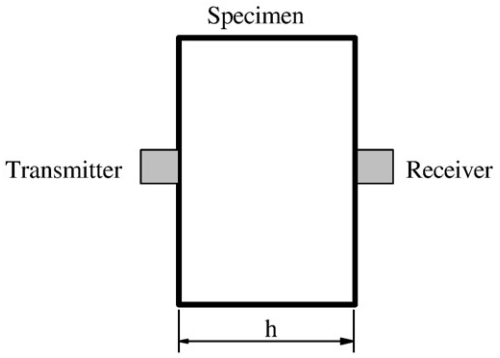

Fig. 10. Ultrasonic wave velocity method.

Based on the principle of strain-equivalence in damage mechanics, the constitutive relation of damaged material is deduced from that of intact material. Therefore, the visco-elastic damage model becomes

$$\sigma = (1-D)\left[f_e(\varepsilon) + E_1\int_0^t \dot{\varepsilon}\exp\left(-\frac{t-\tau}{\theta_1}\right)d\tau + E_2\int_0^t \dot{\varepsilon}\exp\left(-\frac{t-\tau}{\theta_2}\right)d\tau\right] \quad (8)$$

when the strain of the material is very low, the elastic element is approximately linear. Thus,

$$f_e = E_0\varepsilon \quad (9)$$

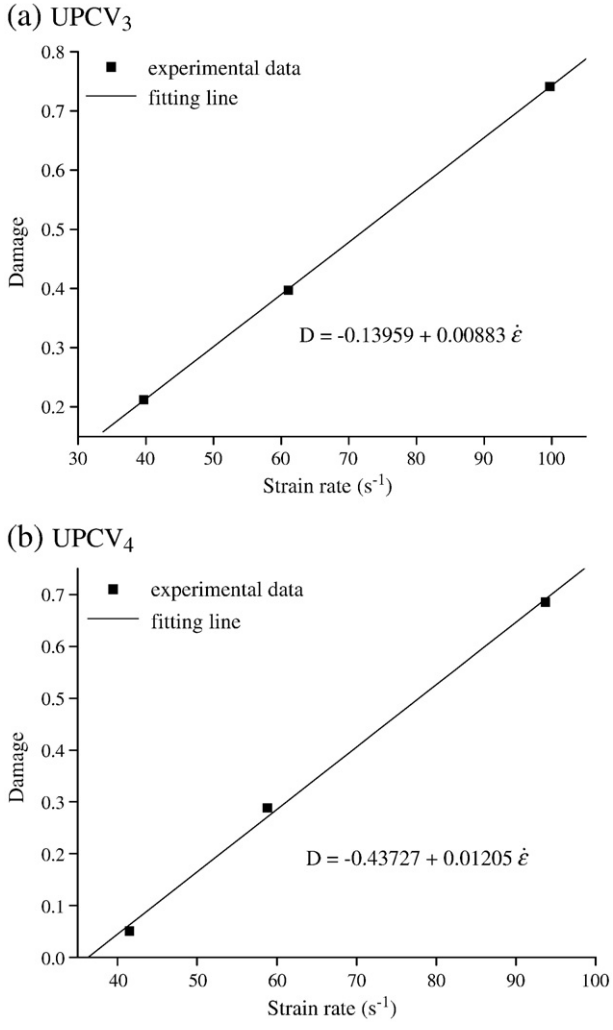

Fig. 11. Relation between the damage and the strain rate of UHPCC on impact.

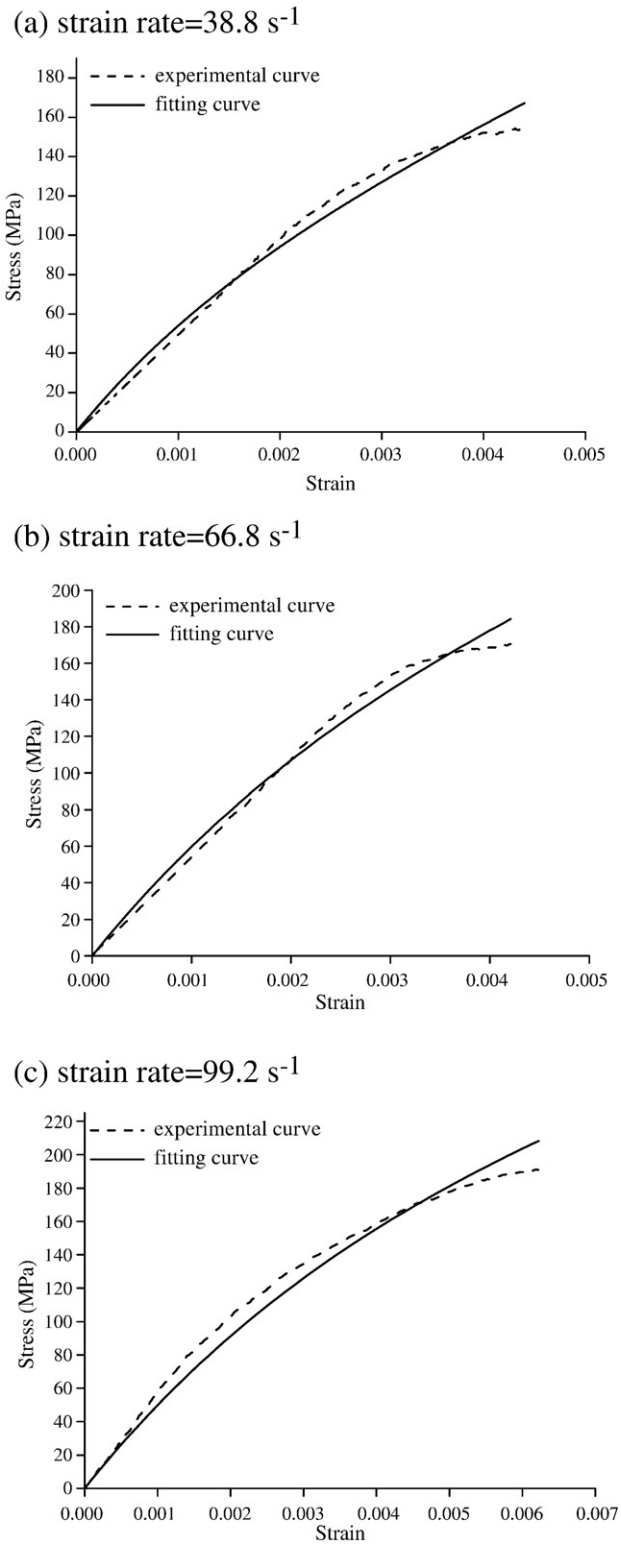

Fig. 12. Comparison between the fitting and experimental stress–strain curves of UPCV3.

As the strain rate $\dot{\varepsilon}$ of the specimen is approximately invariable under impact through SHPB, Eq. (8) becomes

$$\sigma = (1-D)\left[E_0\varepsilon + E_1\varepsilon + E_2\theta_2\dot{\varepsilon}\left(1 - \exp\left(-\frac{\varepsilon}{\dot{\varepsilon}^{\theta_2}}\right)\right)\right] \quad (10)$$

If $E = E_0 + E_1$, Eq. (10) becomes

$$\sigma = (1 - D)\left[E\varepsilon + E_2\theta_2\dot{\varepsilon}\left(1 - exp\left(-\frac{\varepsilon}{\dot{\varepsilon}\,\theta_2}\right)\right)\right] \quad (11)$$

where, E, E_2 and θ_2 are fitting parameters.

Eq. (11) is the visco-elastic damage model of UHPCC. Through nonlinear regress analysis, the fitting stress–strain curves and the experimental curves are shown in Figs. 12, 13. Results show that the theoretical and the experimental data are very similar and the given model is feasible. Table 4 gives the values of the fitting parameters. E and E_2 show elastic properties of concretes at low and high strain rates. θ_2 is relaxation time and it shows viscous properties of concretes at high strain rates. Table 4 indicates that E_1 and E_2 increase with strain rate increasing. D is dynamic damage of concretes and it increases linearly with strain rate. The damage of UHPCC can be calculated using the equations shown in Fig. 11.

Table 4
Values of the fitting parameters.

Materials	$UPCV_3$			$UPCV_4$		
Strain rate(s^{-1})	38.8	66.8	99.2	23.7	44.0	95.8
E (GPa)	31.3	35.2	44.2	32.0	37.1	39.8
E_2 (GPa)	49.3	88.0	163.9	35.6	38.5	214.3
θ_2 (μs)	40.0	40.0	40.0	30.0	30.0	30.0

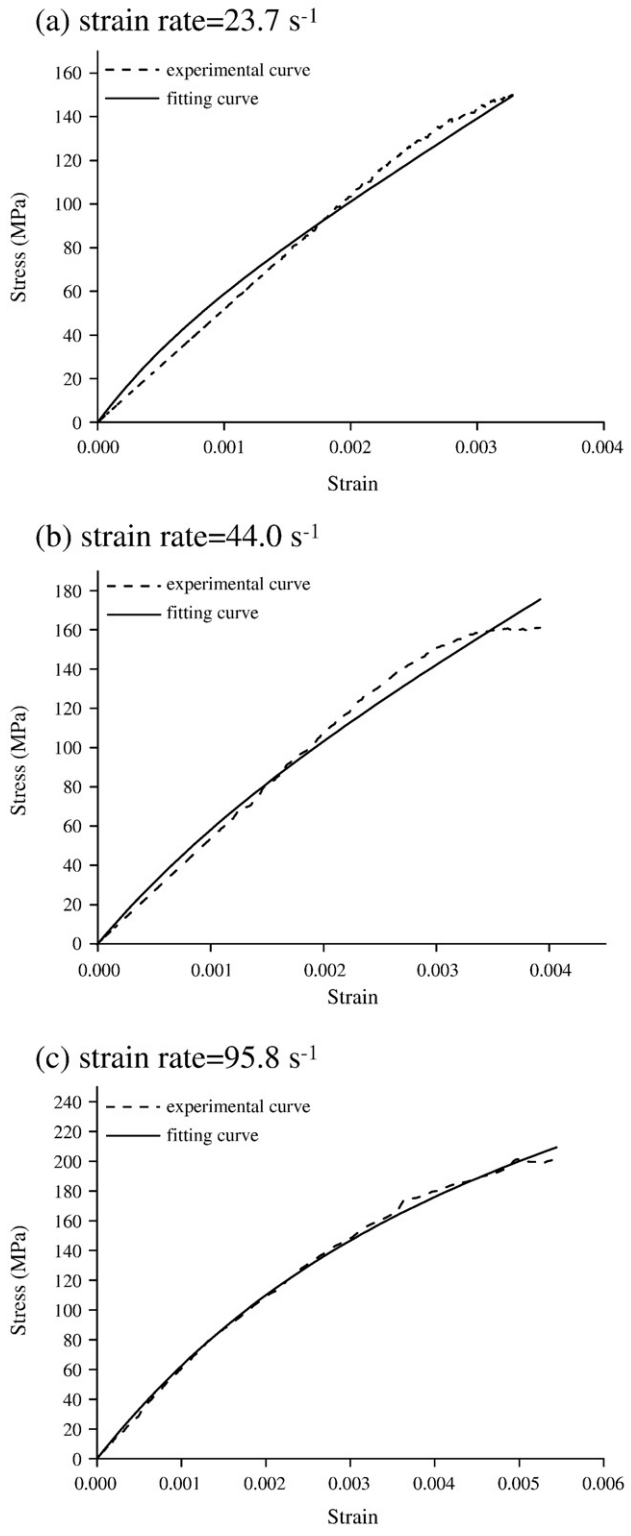

Fig. 13. Comparison between the fitting and experimental stress–strain curves of UPCV4.

The nonlinear visco-elastic model (Eq. (3)) can be deduced from the multi-integral constitutive theory introduced by Green and Rivlin [14,17]. It can be applied to static and dynamic tests using different equipments. Eq. (11) includes damage and is deduced from Eq. (3) on the assumption that material strain is low and strain rate is invariable.

6. Conclusion

The peak stress, peak strain and elastic modulus of UHPCC increase with increasing strain rate. The effects of steel fibers are greater on the toughness than on the strength of UHPCC. The strain rate sensitivity of concrete is ascribed to two causes: the time-dependent movement of free water through voids and pores, and the time-dependent nature of crack growth relative to the load rate. The conclusion that the ability of impact resistance of UHPCC is improved by fiber reinforcement can be drawn by comparing the different fracture patterns of unreinforced and reinforced specimens. The visco-elastic damage model of UHPCC is established based on ZWT model and the material damage measured by ultrasonic wave velocity method.

Acknowledgements

This work is supported by National Natural Science Foundation of China (no. 50808101), Jiangsu Provincial Program for Basic Research (Natural Science Foundation) (no. BK2008417) and China Postdoctoral Science Foundation (no. 20080431100). The authors would like to thank Shisheng Hu (University of Science and Technology of China), Xutao Wu and Yiping Meng (Hefei University of Technology, China) for the help in the SHPB test.

References

[1] M.C. Tang, High performance concrete—past, present and future, in: M. Schmidt, E. Fehling, C. Geisenhansluke (Eds.), Ultra High Performance Concrete, Kassel University Press, Kassel, 2004, pp. 3–9.
[2] R. Jacques, L. Cete, First recommendation for ultra-high-performance concrete and example of application, in: M. Schmidt, E. Fehling, C. Geisenhansluke (Eds.), Ultra High Performance Concrete, Kassel University Press, Kassel, 2004, pp. 79–90.
[3] O. Bonneau, C. Poulin, J. Dugat, Reactive powder concrete: from theory to practice, Concrete International 18 (4) (1996) 47–49.
[4] P. Richard, M. Cheyrezy, Composition of reactive powder concrete, Cement and Concrete Research 25 (7) (1995) 1501–1511.
[5] D.L. Grote, S.W. Park, M. Zhou, Dynamic behavior of concrete at high strain rates and pressures: I. Experimental characterization, International Journal of Impact Engineering 25 (2001) 869–886.
[6] C.A. Ross, J.W. Tedesco, S.T. Kuennen, Effects of strain rate on concrete strength, ACI Materials Journal 92 (1) (1995) 37–47.
[7] M. Sidney, Y. Francis, D. David, Concrete, Pearson Education Inc., New Jersey, 2003.
[8] W.F. Bracc, A.H. Joncs, Comparison of uniaxial deformation in shock and static loading of three rocks, Geoph Res 76 (20) (1971) 4913–4921.
[9] W. Janach, The role of bulking in brittle failure of rocks under rapid compression, International Journal of Rock Mechanics and Mining Sciences 13 (6) (1976) 177–186.

[10] D.A. Gorham, Specimen inertia in high strain-rate compression, Journal of Physics D 22 (1989) 1888–1893.
[11] D.Y. Gao, J.X. Liu, Basic Theory of Steel Fibre Reinforced Concrete, Science and Technology Literature Press, Beijing, 1994.
[12] C.H. Chu, L.L. Wang, D.B. Xu, A nonlinear thermo–viscoelastic constitutive equation for thermoset plastics at high strain rates, in: W.Z. Chien (Ed.), Proceedings of the International Conference on Nonlinear Mechanics, Shanghai, China, 1985, pp. 92–97.
[13] L.L. Wang, D.J. Huang, S. Gan, Nonlinear viscoelastic constitutive relations and nonlinear viscoelastic wave propagation for polymers at high strain rates, in constitutive relation in high/very high strain rates, in: K. Kawata, J. Shioiri (Eds.), IUTAM Symposium, Noda, Japan, 1995, pp. 137–146.
[14] L.L. Wang, Foundation of Stress Waves, National Defense Industry Press, Beijing, 2005.
[15] J. Lemaitre, J.L. Chaboche, Mechanics of Solid Materials, Cambridge University Press, Cambridge, 1990.
[16] P.K. Mehta, P.J.M. Monteiro, Concrete: Microstructure, Properties, and Materials, McGraw-Hill, New York, 2006.
[17] A.E. Green, R.S. Rivlin, The mechanics of nonlinear materials with memory, part I, Archive for Rational Mechanics and Analysis 1 (1957) 1–21.